02

Study of vibrational spectra and thermal behavior of crystallohydrates $Cs_5Zr_4F_{21} \cdot 3H_2O$ and $Rb_5Zr_4F_{21} \cdot 3H_2O$

© N.A. Didenko, E.I. Voit¶

Institute of Chemistry, Far East Branch, Russian Academy of Sciences, Vladivostok, Russia

¶e-mail: evoit@ich.dvo.ru

Received May 13, 2025
Received February 26, 2025
Accepted March 13, 2026

The structure and thermal behavior of isostructural cesium and rubidium crystallohydrates of the composition $Cs_5Zr_4F_{21} \cdot 3H_2O$ and $Rb_5Zr_4F_{21} \cdot 3H_2O$ were studied by vibrational spectroscopy (IR and Raman), DTA-TGA and X-ray diffraction (XRD). Experimental IR and Raman spectra of the $Cs_5Zr_4F_{21} \cdot 3H_2O$, $Rb_5Zr_4F_{21} \cdot 3H_2O$ crystal hydrates and its products thermal dehydration were performed, systematized and analyzed. Based on the results of quantum-chemical calculations, bands in the experimental spectra were assigned. The structural features of the compounds under discussion were considered and differences in the organization of the crystal structures were revealed.

Keywords: complex zirconium fluorides, crystallohydrates of rubidium and cesium fluoridozirconates, vibrational spectroscopy.

DOI: 10.61011/0000000000

Introduction

Rubidium and caesium (along with potassium) are *s* elements of the potassium subgroup. In terms of ionic radius, the cation Cs^+ ($r = 1.88$ Å, coordination number (CN) 12) is closest to the ion Rb^+ ($r = 1.72$, CN 12) [1], and this determines the isomorphism of some caesium and rubidium compounds. Thus, in the family of hexafluorocyanates with the general formula M_2ZrF_6 ($M = Li^+$, Na^+, K^+, Rb^+, Cs^+, NH_4^+, Tl^+), hexasols Rb^+ and Cs^+ are isostructured to each other [2]. At the same time, rubidium and caesium hexafluorocyrconates differ in structure and properties from both a similar compound with potassium ($r = 1.64$ Å, CN 12) and an ammonium cation ($r = 1.43$ Å). Unlike the crystal structures K_2ZrF_6 [3,4] and $(NH_4)_2ZrF_6$ [5,6], which have a polymer chain structure, the structures Rb_2ZrF_6, Cs_2ZrF_6 [2] contain isolated octahedral complex anions $[ZrF_6]^{2-}$.

In the synthesis of fluoride zirconates from aqueous fluoride solutions, under certain conditions, in the case of a lack of fluorine atoms to saturate the coordination capacity of zirconium ($F/Zr < 6$), H_2O molecules interact with the central atom to form multi-ligand aquafluoride complexes. Due to their small size and the ability to form multidirectional hydrogen bonds, both as a donor and as an acceptor of hydrogen bonds, water molecules play an important role in the structural packaging of crystalline hydrates.

The involvement of neutral molecular ligands H_2O into the coordination sphere of the Zr atom occurs at the ratios $F/Zr = 4-5.5$ in known structures of aquafluorocyanates, such as $ZrF_4 \cdot 3H_2O$ [7], $ZrF_4 \cdot H_2O$ [8], $MZrF_5 \cdot H_2O$ ($M = K^+$, NH_4^+, Cs^+) [9–11], $NH_4ZrF_5 \cdot 0.75H_2O$ [6], $Cs_5Zr_4F_{21} \cdot 3H_2O$ [12], $Rb_{9-x}(NH_4)_xZr_6F_{33} \cdot 4H_2O$ [13].

$Rb(Cs)_5Zr_4F_{21} \cdot 3H_2O$ ($F/Zr = 5.25$, $H_2O/Zr = 0.75$, $F + H_2O/Zr = 6$) crystallohydrates were synthesized in the result of interaction of RbF(CsF) and $(H_3O)_2ZrF_6$ in an aqueous solution. Rubidium fluoridohaphnate $Rb_5Hf_4F_{21} \cdot 3H_2O$ was also obtained. The X-ray parameters of the obtained compounds are given [14]. In this case, only the crystal structure of $Cs_5Zr_4F_{21} \cdot 3H_2O$ being one of the representatives of the isotypic series has been determined [12].

The structural features of the $Rb(Cs)_5Zr_4F_{21} \cdot 3H_2O$ compounds under consideration include the union of Zr polyhedra into a tetrameric chain complex anion $ZrF_7-ZrF_7(H_2O)-ZrF_7(H_2O)-ZrF_6(H_2O)$, containing three types of zirconium polyhedra of different composition with different configurations and different Zr CN of 7, 8. $M_5Zr_4F_{21} \cdot 3H_2O$ crystallohydrates are characteristic only of rubidium and caesium and are not formed with other monovalent cations K^+ and NH_4^+.

It should be noted that vibrational spectroscopy data for trihydrates are not presented in any of the well-known reference books, atlases and databases of inorganic compounds.

The isolated IR spectra of $M_5Zr_4F_{21} \cdot 3H_2O(M = Rb^+, Cs^+)$ published so far are given without a detailed description [14,15]. This does not provide a complete picture of the patterns of structural organization of both the compounds under study and other fluoridozirconates containing similar tetrameric fragments. It should be noted that the IR spectra and X-ray diffraction pattern for compounds $RbZrF_5 \cdot H_2O$ and $CsZrF_5 \cdot H_2O$ shown in the atlas [16] correspond to compounds $Rb_5Zr_4F_{21} \cdot 3H_2O$ and $Cs_5Zr_4F_{21} \cdot 3H_2O$.

In order to clarify, supplement, systematize and generalize data on the structure and thermal stability of rubidium

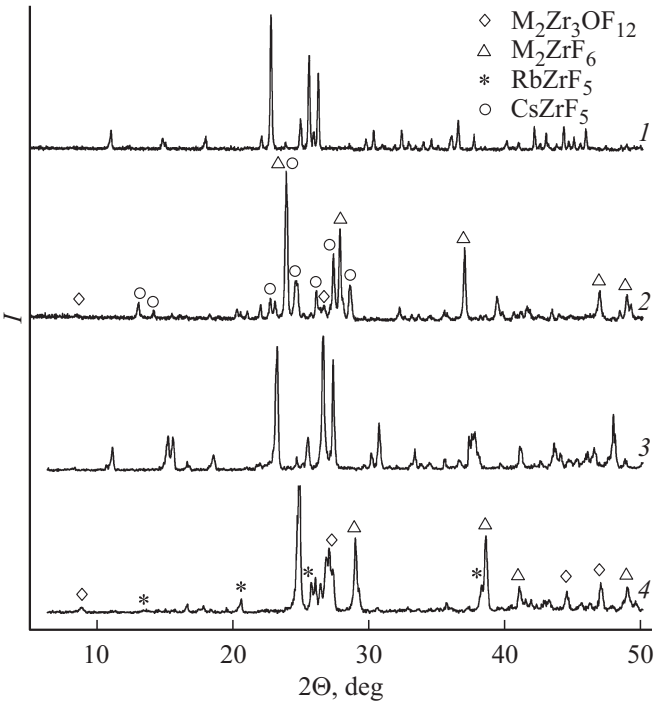


Figure 1. X-ray patterns of compounds $Cs_5Zr_4F_{21} \cdot 3H_2O$ (*1*), $Rb_5Zr_4F_{21} \cdot 3H_2O$ (*3*) and their and corresponding to them products of heating up to 330 °C (*2*), 350 °C (*4*).

and cesium fluoridozirconate crystallohydrates of the composition $M_5Zr_4F_{21} \cdot 3H_2O$, their complex investigation by vibrational (IR, Raman) spectroscopy and thermal analysis was carried out in this work. The interpretation of the spectra is based on quantum chemical calculations.

Experimental part

Compounds $Rb(Cs)_5$ $Zr_4F_{21} \cdot 3H_2O$ were synthesized from a reaction mixture of $ZrO(NO_3)_2 \cdot 2H_2O$ and MF (at a molar ratio of 1:1) in an aqueous solution of hydrofluoric acid. 5.34 g of zirconyl nitric acid 2-water (bha. $\geq$ 99 %, 0.02 mol) is dissolved in a mixture of 10 ml H_2O and 4 ml 40 % HF (ultra high purity 99.99 %) at room temperature. An aqueous solution of rubidium fluoride 2.09 g (0.02 mol) or caesium fluoride 3.04 g (0.02 mol) in 20 ml H_2O (in the presence of several drops of dilute acid HF) was added to the resulting solution. $Rb(Cs)_5Zr_4F_{21} \cdot 3H_2O$ crystalline precipitates from such systems occurs within a few days. The single-phase nature of the obtained compounds was confirmed by the XRD method (Fig. 1). X-ray patterns of synthesized crystallohydrates $Cs_5Zr_4F_{21} \cdot 3H_2O$ (mapPDF-2.№01-077-0841(C)) and $Rb_5Zr_4F_{21} \cdot 3H_2O$ are similar (Fig. 1, curves *1*, *3*). The compounds crystallize in monoclinic syngony with similar unit cell parameters [14].

X-ray diffraction data for the synthesized compounds were obtained using a Bruker D8 ADVANCE diffractometer (CuK_α radiation, graphite monochromator). The powder data bank PDF-2 was used to obtain information about the composition of the products.

The synthesized compounds $Rb(Cs)_5Zr_4F_{21} \cdot 3H_2O$ were heated using a Q-1000 MOM derivatograph in the air atmosphere at a heating rate of 5 deg/min. The sample weights were 331 and 241 mg, respectively, for Cs and Rb salts. Al_2O_3 is used as a reference.

IR spectra were recorded in the 4000−400 cm^{-1} range at room temperature using the IR-Affinity device on the KRS-5 window from samples prepared as a suspension in petroleum jelly. The Raman spectra of the studied compounds were recorded using an RFS100/S spectrometer (Nd:YAG, $\lambda = 1064$ nm laser) with a resolution of 4 cm^{-1}.

To assign bands in the spectra of a number of studied caesium and rubidium crystallohydrates ($Cs_5Zr_4F_{21} \cdot 3H_2O$, $Rb_5Zr_4F_{21} \cdot 3H_2O$), quantum chemical calculations were performed using the GAMESS software package [17]. The calculations were performed in terms of the local density functional theory in combination with the B3lyp exchange-correlation potential. The LANL2DZ basis set with the core potential was used for Zr(IV) and Cs atoms, and the 631-G(dp) basis set, for F, O and H atoms. The selection of model clusters was carried out taking into account the known structural data. The calculation of the equilibrium geometry and the normal vibration frequencies is carried out in the harmonic approximation. The equilibrium geometry and normal vibration frequencies were calculated in the harmonic approximation. The results were obtained using the equipment of the Center „Far-Eastern Computing Resource“ at the Institute of Automation and Control Processes, Far-East Branch of the Russian Academy of sciences (https://cc.dvo.ru).

Results and discussion

Crystal structure, thermal analysis

$Cs_5Zr_4F_{21} \cdot 3H_2O$. According to the XRD data, the compound $Rb_5Zr_4F_{21} \cdot 3H_2O$ is isostructurally similar to the Cs analog of monoclinic syngony (space group $P2_1/m$, $Z = 2$). The lattice cell parameters are equal, respectively, for $Cs_5Zr_4F_{21} \cdot 3H_2O$: $a = 15.088(9)$, $b = 12.614(8)$, $c = 6.798(2)$ Å, $\gamma = 108.08(5)°$ [12] and for $Rb_5Zr_4F_{21} \cdot 3H_2O$: $a = 14.82$, $b = 12.06$, $c = 6.47$ Å, $\gamma = 106.6°$ [14].

The crystal structure of $Cs_5Zr_4F_{21} \cdot 3H_2O$ is constructed from Cs^+ cations and tetrameric anions $[Zr_4F_{21}(H_2O)_3]^{5-}$]. The Zr polyhedra (CN 7 and 8) are connected by common edges F-F in tetra-corefragments $ZrF_7-ZrF_7(H_2O)-ZrF_7(H_2O)-ZrF_6(H_2O)$. The simultaneous existence in the tetramer of two Zr polyhedra of different compositions with a CN 7 makes it possible for a comparative assessment of their distortions, characterized by a spread of distances Zr-F, Zr-O and valence angles. The CN of Cs^+ cations is 12. In the interval 4 Å $Cs(1)^+$ cations are surrounded by eight F atoms and four O atoms, $Cs(2)^+$ cations are surrounded by eleven F atoms and one

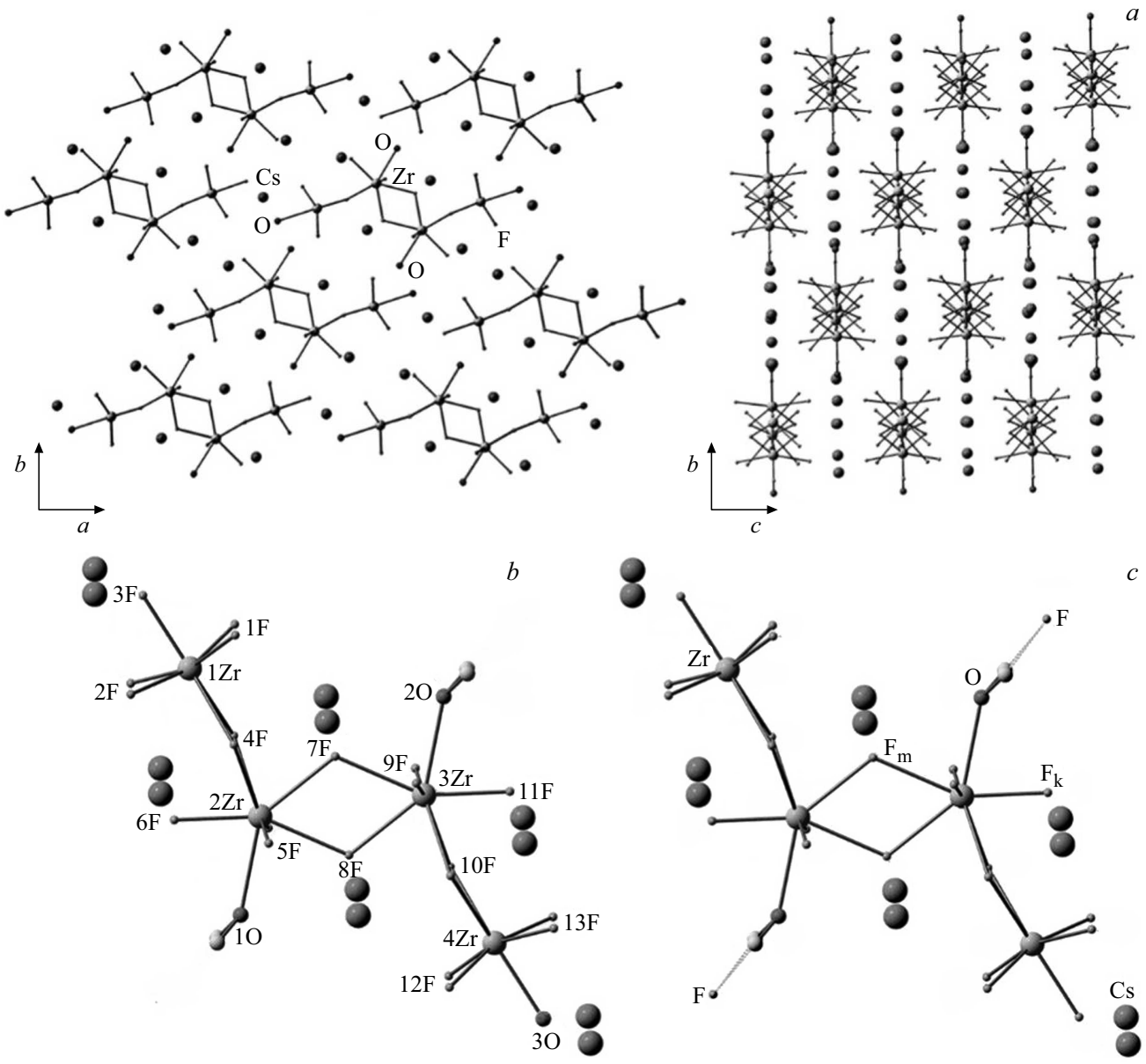


Figure 2. Projections of the $Cs_5Zr_4F_{21} \cdot 3H_2O$ crystal structure in the *ab* and *bc* planes (*a*). The $[Zr_4F_{21}(H_2O)_3]^{5-}$ complex anion in the structure (*b*) and the model $[Zr_4F_{22}(H_2O)_2]^{6-}$ (C_{2h}) anion (*c*) in a cationic environment.

O atom, and $Cs(3)^+$, $Cs(4)^+$ and $Cs(5)^+$ — with twelve atoms F. The projections of the $Cs_5Zr_4F_{21} \cdot 3H_2O$ structure are shown in Fig. 2, *a*.

Thermal dehydration $Cs_5Zr_4F_{21} \cdot 3H_2O$ begins at 95 °C and proceeds in one stage with a maximum rate at 130 °C (Fig. 3, *a*). The decrease in mass at 200 °C is 3.7 % (when splitting off three molecules H_2O $\Delta m_{calc} = 3.64$ %). According to XRD, IR and Raman spectroscopy data, as a result of dehydration of $Cs_5Zr_4F_{21} \cdot 3H_2O$, a mixture of two phases $CsZrF_5$ (map No. 00-011-0082(N)) and Cs_2ZrF_6 (map No. 01-074-0173(C)) is formed, which is described by the general reaction

$$Cs_5Zr_4F_{21} \cdot 3H_2O \rightarrow 3CsZrF_5 + Cs_2ZrF_6 + H_2O.$$

It is likely that the weakening of cation-anion interactions and the increase in dynamic processes in both sublattices of the $Cs_5Zr_4F_{21} \cdot 3H_2O$ structure with increasing temperature lead to simultaneous dehydration and disproportionation reactions in fluorine and cation. As a result, two thermally more stable compounds $CsZrF_5$ and Cs_2ZrF_6 are formed.

Upon further heating of $Cs_5Zr_4F_{21} \cdot 3H_2O$ above 200 °C, a narrow intense endothermic effect is recorded on the differential thermal analysis curve at 320 °C, corresponding to the reversible phase transformation (PT) of $CsZrF_5$, which is consistent with the data from [18]. The decrease in mass increases wightly in the temperature range of PT and amounts to 4.5 % at 330°, which is associated with the onset of pyrohydrolysis of $CsZrF_5$ by air moisture and the formation, according to vibrational spectroscopy data, of

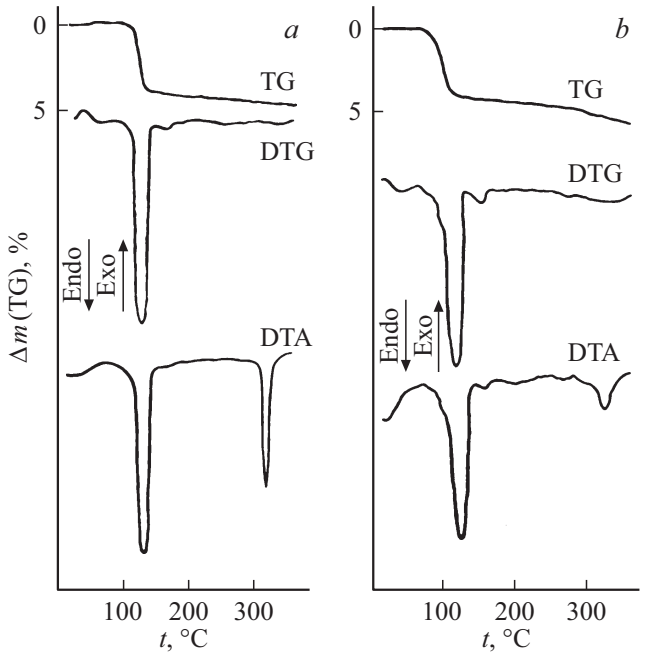


Figure 3. Thermoanalytical curves $Cs_5Zr_4F_{21} \cdot 3H_2O$ (*a*) and $Rb_5Zr_4F_{21} \cdot 3H_2O$ (*b*).

the impurity phase of oxofluorocyrconate $Cs_2Zr_3OF_{12}$ (see below). According to the XRD data, the heating product ($T = 330\,^\circ$C) consists mainly of a mixture of phases $CsZrF_5$ and Cs_2ZrF_6 (Fig. 1, curve *2*).

$Rb_5Zr_4F_{21} \cdot 3H_2O$. Dehydration of $Rb_5Zr_4F_{21} \cdot 3H_2O$ begins at 100 °C and proceeds in one stage with a maximum rate at 135 °C. The decrease in mass at 200 °C is 4.4 % (when splitting off three molecules H_2O $\Delta m_{calc} = 4.34\,\%$).

Upon dehydration, the compound $Rb_5Zr_4F_{21} \cdot 3H_2O$ also decomposes into a mixture of phases $RbZrF_5$ (map No.00-034-0549(Q)) and Rb_2ZrF_6 (map No.01-074-0172(C)). When the sample is heated above 230 °C, a gradual decrease in mass begins, associated with partial pyrohydrolysis of $RbZrF_5$ with moisture from the air to form the phase $Rb_2Zr_3OF_{12}$ (space group $R\bar{3}m$) [19], isostructural to compounds $M_2Zr_3OF_{12}$ ($M{-}K^+$, Rb^+, Tl^+, NH_4^+) [20]. The endopic corresponding to PT $\alpha \leftrightarrow \beta$ $RbZrF_5$ is detected at 330 °C. The decrease in mass at 350 °C is 5.8 % (Fig. 3, *b*). An X-ray pattern of the product heated to 350 °C is shown in Fig. 1, curve *4*.

It should be noted that according to XRD data, the resulting rubidium and caesium salts $MZrF_5$, obtained by decomposition of $M_5Zr_4F_{21} \cdot 3H_2O$, are not isostructural with each other. The $RbZrF_5$ compound is a triclinic modification (space group $P\bar{1}$, $Z = 6$), isostructural to the K-analog with a layered structure [21]. The refined lattice cell parameters for $RbZrF_5$ are also presented in this paper, which differ from the data of the map №00-034-0549(Q) and the publication [22]. For the low-temperature phase $CsZrF_5$, only the interplane distances are known without specifying the crystallographic characteristics [23]. The comparison shows a certain similarity between radiographs of caesium pentafluoridozirconate and $TlZrF_5$ (Tl^+, $r = 1.70$ Å, CN 12). The $TlZrF_5$ compound crystallizes in monoclinic syngony (space group $P2_1/c$, $Z = 4$) [24] and has an anion layer structure different from that in the $KZrF_5$, $RbZrF_5$ structures.

Thus, according to thermal analysis and XRD data, isostructured crystallohydrates $Cs(Rb)_5Zr_4F_{21} \cdot 3H_2O$ have similar dehydration temperatures, the same composition of their thermal decomposition phases during dehydration (a mixture of M_2ZrF_6 and $MZrF_5$) and the same character of thermal decomposition of the $MZrF_5$ phase when interacting with water and air vapors to form oxofluorozirconate $M_2Zr_3OF_{12}$. At the same time, the tendency to pyrohydrolysis in rubidium pentafluorocyrconate is more pronounced than in the corresponding phase with the caesium cation. The presence of $Cs_5Zr_4F_{21} \cdot 3H_2O$ ($T = 330\,^\circ$C) oxofluoridozirconate $Cs_2Zr_3OF_{12}$ in the calcination product has been established for the first time.

Vibrational Spectroscopy of $Cs(Rb)_5Zr_4F_{21} \cdot 3H_2O$

The vibrational spectra of the trihydrates $Cs_5Zr_4F_{21} \cdot 3H_2O$ (spatial group $P2_1/m$, $Z = 2$) and $Rb_5Zr_4F_{21} \cdot 3H_2O$ are similar (Fig. 4), which confirms the isostructure of the studied compounds.

The vibrational spectra of $Cs_5Zr_4F_{21} \cdot 3H_2O$ (space group $P2_1/m$, $Z = 2$) and $Rb_5Zr_4F_{21} \cdot 3H_2O$ trihydrates are similar (Fig. 4), which confirms the isostructural nature of the studied compounds

In the IR spectrum of $Cs_5Zr_4F_{21} \cdot 3H_2O$, a wide valence band of νOH with a maximum of $\sim 3280\,cm^{-1}$, a composite deformation band of δH_2O with maxima of ~ 1685 and $1614\,cm^{-1}$, and a libration band of $\delta_{lib}H_2O$ $\sim 740\,cm^{-1}$ (Fig. 4, *a*, curve *1*). Similar bands in the spectrum of $Rb_5Zr_4F_{21} \cdot 3H_2O$ lie at 3220, 1708, 1634, $822\,cm^{-1}$ (Fig. 4,*b*, curve *1*). The additional maximum with a frequency at $1549\,cm^{-1}$ in the Rb trihydrate spectrum should be attributed to molecular H_2O in the form of inclusions (capture of the mother liquor during crystal formation [25]). The intensity of this band increases in the spectra of larger crystals $Rb_5Zr_4F_{21} \cdot 3H_2O$. The same band is present in the IR spectrum $Rb_5Zr_4F_{21} \cdot 3H_2O$, given in Ref. [15,16].

Thus, the position of the IR vibration bands of H_2O molecules indicates the formation of stronger H bonds in the $Rb_5Zr_4F_{21} \cdot 3H_2O$ structure than in $Cs_5Zr_4F_{21} \cdot 3H_2O$. In the crystal lattice of $Cs_5Zr_4F_{21} \cdot 3H_2O$, coordinated molecules of H_2O, which are part of polyhedra $[ZrF_7(H_2O)]$, participate in the formation of two H-bonds (with distances $O\cdots F$ 2.62 and 2.67 Å) with the formation of layers of anions. A longer H-bonds $OH\cdots F$ 2.82 Å are realized between oxygen atoms and terminal fluorine atoms of neighboring anion layers.

Quantum chemical calculations were performed to assign bands of the anion sublattice in the experimental spectra $M_5Zr_4F_{21} \cdot 3H_2O$ ($M = Cs^+$, Rb^+) located at frequencies below $600\,cm^{-1}$.

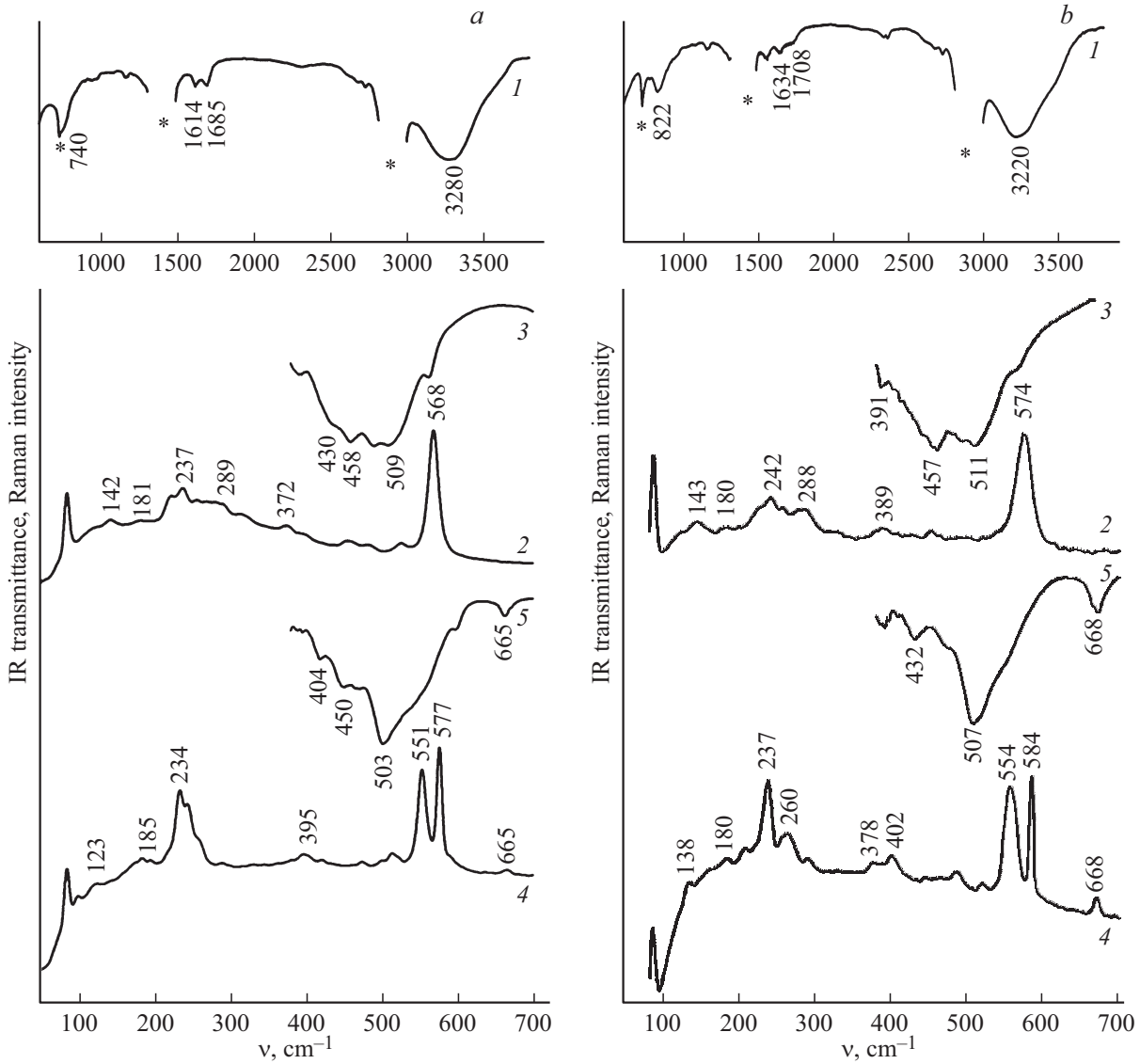


Figure 4. IR- (*1*, *3*, *5*) and Raman (*2*, *4*) spectra of $Cs_5Zr_4F_{21} \cdot 3H_2O$ (*a*), $Rb_5Zr_4F_{21} \cdot 3H_2O$ (*b*) compounds and products of their thermal decomposition.

Despite the fact that the crystal structure of $Cs_5Zr_4F_{21} \cdot 3H_2O$ is formed by complex anions $[Zr_4F_{21}(H_2O)_3]^{5-}$ which can be considered a „natural" object for modeling, a centrosymmetric tetrameric anion $[Zr_4F_{22}(H_2O)_2]^{6-}$ was chosen in this paper for calculating oscillatory frequencies (Fig. 2, *b*, *c*). With this choice, the cluster has a point symmetry C_{2h}, and the replacement of one H_2O molecule with an atom of F leads to minor differences in the calculated data compared with the structural ones (Table 1). Increasing the local symmetry of the anion makes it possible to reduce the calculation time, simplify, unify, and visually represent the band assignments in which each of the modes is symmetrical (Table 2).

Initially, the optimal geometry of the cluster was found $[Cs_{12}Zr_4F_{24}(H_2O_2)]^{4+}$ (C_{2h}) with Cs^+ outer sphere cations and two „external" F atoms frozen in crystallographic positions (Fig. 2, *c*). The optimized geometric parameters of the tetra-core fragment of the composition $[Zr_4F_{22}(H_2O)_2]$ surrounded by cations are in satisfactory agreement with the structural data (Table 1). The vibrational frequencies of the tetrameric grouping $[Zr_4F_{22}(H_2O)_2]^{6-}$ are calculated in the equilibrium geometry (Table 2).

Based on the data obtained, the vibrational spectrum of the tetrameric anion $[Zr_4F_{22}(H_2O)_2]^{6-}$ (C_{2h}), excluding protons vibrations, is described by the irreducible representation

$$\Gamma_{C2h} = 23\mathrm{Ag(RS)} + 22\mathrm{Bu(IR)} + 17\mathrm{Au(IR)} + 16\mathrm{Bg(RS)}.$$

The calculated vibrational frequencies are grouped by the predominant contributions to each vibration (Table 2). It can be seen that similar frequencies represent a set (group) of possible symmetric and asymmetric combinations of characteristic oscillations of Zr polyhedra. The images of the main most active IR and Raman vibrations are shown in Fig. 5.

Table 1. Geometric parameters of anions in the $Cs_5Zr_4F_{21} \cdot 3H_2O$ structure and in the equilibrium geometry of the $[Cs_{12}Zr_4F_{24}(H_2O_2)]^{4+}$ (C_{2h}) model cluster

Structural data $[Zr_4F_{21}(H_2O)_3]^{5-}$		Calculated data $[Zr_4F_{22}(H_2O)_2]^{6-}$ (C_{2h})
Distances	Zr-F, Å	Zr-F, Å
Zr1-Zr2, Zr3-Zr4	3.668 (1), 3.601(1)	3.791
Zr2-Zr3	3.662(1)	3.790
Zr1-F4, Zr4-F10	2.150(5), 2.093(5)	2.280
Zr1-F3	2.043(8)	2.007
Zr2-F7, Zr3-F8	2.118(0), 2.107(9)	2.222
Zr3-F7, Zr2-F8	2.255(9), 2.243(9)	2.240
Zr2-F5, Zr3-F9	1.993(5), 1.999(5)	2.078
Zr2-F6, Zr3-F11	1.970(9), 1.982(9)	1.984
Zr2-F4, Zr3-F10	2.212(4), 2.227(9)	2.212
Zr2-O1, Zr3-O2	2.332(9), 2.270(9)	2.301
Zr4-O3	2.316(9)	–
Zr1-F2, Zr4-F13	2.053(6), 1.992(7)	2.024
Zr1-F1, Zr4-F12	2.019(6), 2.033(6)	2.075
Angles	ω, °	ω, °
F1-Zr1-F2, F12-Zr4-F13	94.5(4), 91.9(3)	89.939
F1-Zr1-F4, F10-Zr4-F12	75.8(3), 77.9(3)	74.116
F2-Zr1-F4, F10-Zr4-F13	75.6(3). 78.7(2)	76.675
F4-Zr2-F5, F9-Zr3-F10	139.0(4), 137.8(3)	136.445
F4-Zr2-F6, F10-Zr3-F11	77.1(3), 75.3(3)	78.047
F4-Zr2-F8, F7-Zr3-F10	127.6(4), 128.6(3)	122.814
F5-Zr2-F6, F9-Zr3-F11	92.8(3), 95.2(3)	94.797
F5-Zr2-F8, F7-Zr3-F9	78.9(3), 77.9(4)	80.139
F6-Zr2-F7, F8-Zr3-F11	145.3(3), 144.2(3)	143.680
F6-Zr2-O1, F11-Zr3-O2	77.4(5), 76.7(4)	76.459
F6-Zr2-F8, F7-Zr3-F11	149.1(4), 149.8(3)	153.947
F5-Zr2-F7, F8-Zr3-F9	97.1(3), 94.4(3)	93.570
F5-Zr2-O1, F9-Zr3-O2	74.2(4), 76.6(5)	78.859
F4-Zr2-O1, F10-Zr3-O2	138.6(5), 136.9(4)	136.852
F3-Zr1-F4, F10-Zr4-O3	146.8(4), 145.7(5)	148.604
F1-Zr1-F3, F12-Zr4-O3	80.0(3), 77.8(4)	84.609
F2-Zr1-F3, F13-Zr4-O3	84.0(3), 78.2(4)	80.686
F8-Zr2-O1, F7-Zr3-O2	71.7(4), 73.1(4)	74.825
F4-Zr2-F7, F8-Zr3-F10	73.5(3), 74.4(3)	72.898
F5-Zr2-F7, F8-Zr3-F9	97.1(3), 94.4(3)	93.722
F7-Zr2-F8, F7-Zr3-F8	65.5(3), 65.8(4)	63.710
F7-Zr2-O1, F8-Zr3-O2	138.9(4), 137.2(4)	138.535
Zr2-Zr3-Zr4	108.452	107.984

According to the calculation results, symmetric (Ag) combinations of vibrations are the most intense in the Raman spectrum of the model tetramer. In the experimental Raman spectrum of $Cs_5Zr_4F_{21} \cdot 3H_2O$, the most intense and broadened peak $\sim 568\,cm^{-1}$ can be attributed to to fullsymmetrical stretching of Zr-F bonds of polyhedra with different CN Zr 8 and 7 (calculated frequencies 581 and $577\,cm^{-1}$ symmetry Ag, Fig. 5, *a*, *b*), the largest contribution to this vibration is made by stretching of the terminal bonds (designation $\nu_s ZrF_k$). It is important to note here that in the $C_5Zr_4F_{21} \cdot 3H_2O$ structure in polyhedra $[ZrF_7(H_2O)]$ the shortest terminal bonds Zr-F_k (1.982, 1970 Å) were determined, as in the calculated equilibrium geometry of the tetramer (Table 1). These Zr-F_k bonds do not participate in the formation of H-bonds. Symmetrical combinations of the stretching vibrations of the terminal bonds $\nu_s ZrF_k$ ($451\,cm^{-1}$, Ag) and the deformation vibration of the bridge bonds δZr_2F_m ($466\,cm^{-1}$, Ag) (Fig. 5, *d*) are localized lower in frequency in the Raman spectrum (Fig. 5, *d*) They are not very intense in the experimental Raman spectrum and according to the calculation results.

According to the data (Table 2), the main contribution of Zr-O bond stretching is present in two sets of modes (420, $416\,cm^{-1}$ Bu, Ag) and (373, $363\,cm^{-1}$ Bu, Ag), representing combinations of ν $Zr(O \pm 2F_m)$. These vibrations

Table 2. Experimental band positions in the spectra of $Cs_5Zr_4F_{21} \cdot 3H_2O$ and $Rb_5Zr_4F_{21} \cdot 3H_2O$, calculated vibrational frequencies of the $[Zr_4F_{22}(H_2O)_2]^{6-}$ anion in the $[Cs_{12}Zr_4F_{24}(H_2O_2)]^{4+}$ cluster, and their assignment.

Experimental spectrum				Calculation $[Zr_4F_{22}(H_2O)_2]^{6-}$		Assignment*
$Cs_5Zr_4F_{21} \cdot 3H_2O$		$Rb_5Zr_4F_{21} \cdot 3H_2O$				
IR	Raman	IR	Raman		Symmetry	
ν, cm^{-1}				ν, cm^{-1}	C_{2h}	
565 av	568 s	571	574	581, 562	Ag, Bu	$\nu_s ZrF_k$ (CN 8) ax
				581, 577	Bu, Ag	$\nu_s ZrF_k$ (CN 7) ax, eq
509 s	525 w	511 s	538	529, 528	Au, Bg	$\nu_{as} ZrF_k$ (CN 7) eq
				506, 505	Bu, Ag	$\nu_{as} ZrF_k$ (CN 7) ax, eq
490 av pl	484 w	493 av pl	502−490 w	488, 485	Bu, Ag	$\nu_s ZrF_k$-Fm (CN 8)
				480, 460	Au, Bg	$\nu_{as} ZrF_k$ (CN 8) (eq)
		460 s	461	466	Ag	$\delta Zr(F_m+F_m)$ (CN 8)
458 s	455 av	453 w	457 av	443, 440	Bu, Ag	$\delta Zr(F_m+F_m)$ (CN 7−8)
				458, 451	Bu, Ag	$\nu_{as} ZrF_k$ (CN 7) ax,eq
				429, 429	Au, Bg	$\nu_s Zr(F_k\text{-}F_k)$ (eq, CN 7)
430 wide av	400		406	420, 416	Bu, Ag	$\nu_{as} Zr(O\text{-}2F_m)$ (CN 8)
392 w	372 wide w	386 w	387 wide w	373, 370	Bu, Ag	$\nu_{as} Zr(2F_m+O)$ (CN 7−8)
				355	Bu	$\nu_{as} Zr2F_m$(CN 8−8)
			344 w	370, 370	Au, Bg	$\nu_{as} Zr(F_m\text{-}F_m)$ (CN 7−8)
				340	Ag	
			330 w	320, 321	Au, Bg	δ//$Zr2F_m$ (CN 7−8)
				341	Bu	δ//$Zr2F_m$ (CN 8)
	315 w		320 w	320, 315	Ag, Bu	δ//$ZrOF_k$ (CN 8)
	289 wide av		288 wide av	300, 280	Au, Bg	ωZrF_kO (CN 8)
				293, 279	Ag, Bu	$\delta_{sc} ZrF_kO$ (CN 8)
				278, 277	Au, Bg	twZrF_m (CN 7−8)
				268	Bg	twZrF_mF (CN 8)
	280 pl			276, 275	Bu, Ag	ωZrF_k (CN 7, 8) ax, eq
	268 w			277, 276	Ag, Bu	ωZrF_k (CN 7, 8) ax, eq
	256 w		256 w	258, 255	Bu, Ag	ωZrF_k (CN 7) ax, eq
				245, 243	Bg, Au	ωZrF_k (CN 7) ax
				235, 228	Bg, Au	$\delta\perp ZrOF_k$
	237 s		242 s	232, 230	Bu, Ag	$\delta_{sc} ZrF_k$ (CN 7)
	223 av		225 w	226, 221	Ag, Bu	γZrF_k (CN 8)
				209−20	4Ag, 5Bu	ρ, tw, lattice
					6Bg, 8Au	
	181, 142		183, 143	193, 142	Ag, Ag	$\nu ZrF_7(H_2O)-ZrF_7(H_2O)$
						$\nu ZrF_7(H_2O)-ZrF_7$

Note: Relative intensities: s — strong, av — medium, w —weak, wide — wide, pl — shoulder. *ν — valence, δ — deformation: δ_{sc} — scissor, ω — wagging, γ — umbrella, tw — twisting, ρ — rocking. //, $\perp$ — along and across the plane of symmetry of the tetramer.

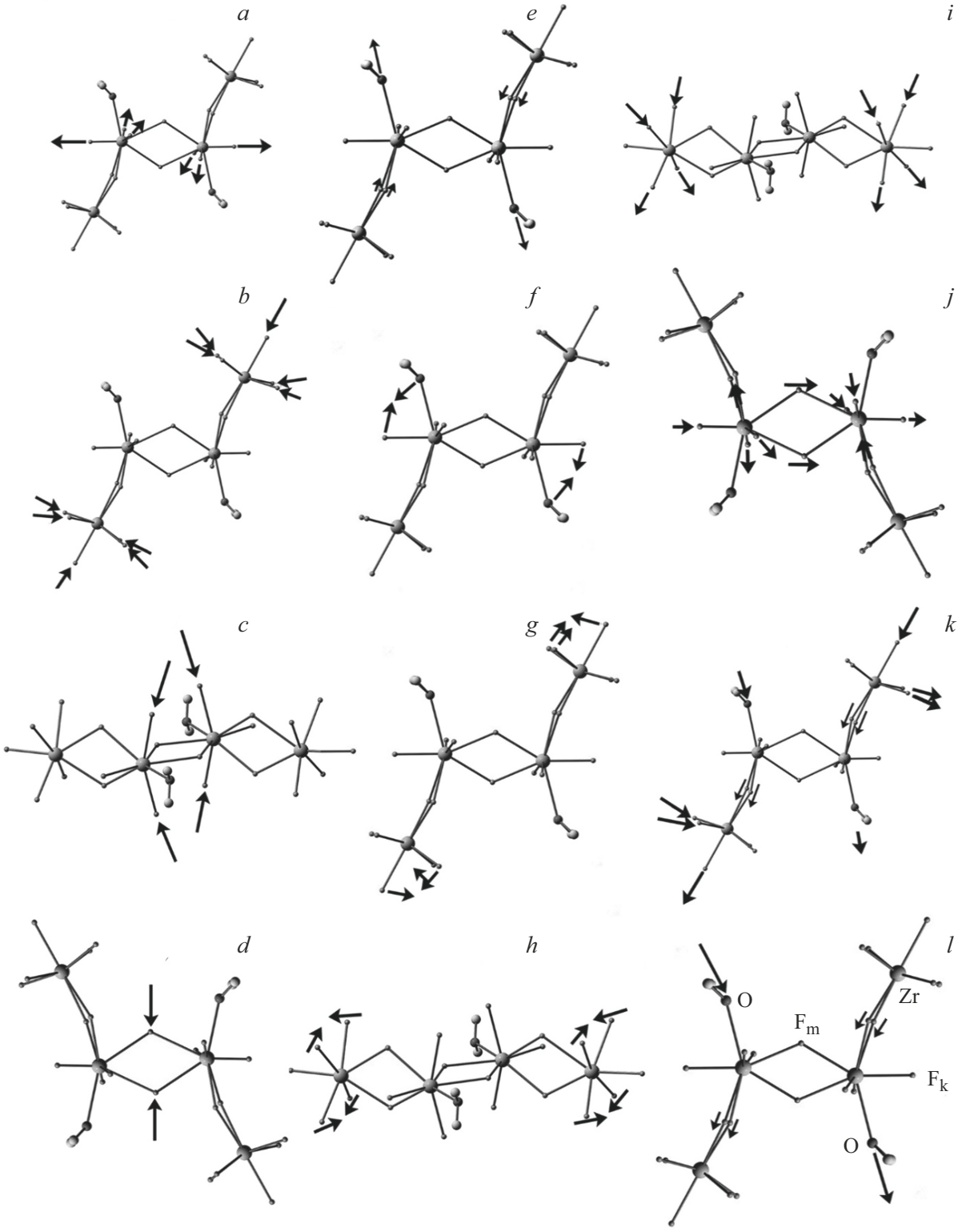


Figure 5. The calculated intensive Raman are (581 (*a*),577 (*b*), 480 (*c*), 466 (*d*), 416 (*e*), 293 (*f*),275 (*g*), 230 (*h*) cm^{-1}) and IR (529 (*i*), 488 (*j*), 458 (*k*),420 (*l*) cm^{-1}) vibrations of anion $[Zr_4F_{22}(H_2O)_2]^{6-}$ (C_{2h}).

are related to the characteristic oscillations of a polyhedron with a Zr CN 8. In the first frequency group $\nu Zr(O\text{-}2F_m)$ increased the contribution of stretching of bonds Zr-O, in the second $\nu Zr(O{+}2F_m)$ — stretching of bridging bonds Zr-$2F_m$. Thus, a composite band of low intensity in the experimental Raman spectrum in the 400−370 cm^{-1} region

corresponds to symmetric combinations of Zr−O bond stretchings (calculated at 416 cm^{-1}, Ag) (Fig. 5, *e*) and Zr−F. stretchings (363 cm^{-1}, Ag).

The main calculated frequencies of bending vibrations of the tetrameric unit are below 330 cm^{-1} (Table 2). The 320−270 cm^{-1} region contains deformation modes involving O atoms, and the 280−220 cm^{-1} range contains the most intense deformation vibrations (ω, sciss, γ) caused by changes in the angles between the terminal bonds F_k-Zr-F_k tetramer (fig. 5, *f*–*h*). All these features (from CN 7, 8 polyhedra) are significantly mixed. Thus, in the experimental Raman spectrum of $Cs_5Zr_4F_{21} \cdot 3H_2O$, the most intense deformation band with a complex contour and several maxima ($\sim$ 289, 280, 268, 256, 237, 223 cm^{-1}) refers to deformation vibrations involving Zr-F_k bonds.

The calculated rocking, twisting, translational and lattice vibrations of the anion are below 200 cm^{-1}. Of these, the modes in the Raman spectrum are the most intense (calculated 193, 142 cm^{-1}), which determine translational movements of Zr polyhedra towards each other in the plane of symmetry in the tetramer. Two bands can be attributed to them at 181 (CN 8) and 142 cm^{-1} (CN 7) in the Raman experiment (Fig. 4, *a*, spectrum *2*).

One of the most intense and broad bands in the experimental IR spectrum of $Cs_5Zr_4F_{21} \cdot 3H_2O$ with a maximum at 509 cm^{-1} (calculated 529 cm^{-1}, Au) can be attributed to valence asymmetric oscillations $\nu_{as}ZrF_k$ with a predominant contribution of stretching of terminal bonds in Zr polyhedra with CN 7 (Fig. 5, *i*). Another maximum at 490 cm^{-1} (488 cm^{-1}, Bu) is determined by an asymmetric combination of symmetric stretching vibrations of all bonds in a polyhedron with CN 8 with an antiphase movement of the short terminal Zr-F_k bond (Fig. 5, *j*). The manifestation of an asymmetric component in the experimental IR spectrum is caused by the forced movement of bridge atoms F_m between polyhedra with CN 8.

The IR band of $\sim$ 458 cm^{-1} is an overlap of several close modes (Table 2), of which the most intense is calculated at 458 cm^{-1}(*Bu*). It is represented by a combination of co-directional stretching of both the terminal bonds of polyhedra with CN 7 and, to a lesser extent, the Zr-O bonds of polyhedra with CN 8 (Fig. 5, *k*). These synchronous asymmetric co-directional stretches of the end bonds of the tetramer cause stretches of the bridging bonds between polyhedra with CN 7 and 8. In addition, it can be assumed that the main contribution of the valence vibration νZrO is in the arm of the experimental IR spectrum $\sim$ 430 cm^{-1} (calculated 420 cm^{-1}, Bu, Fig. 5, *l*).

Comparing the very similar experimental spectra of the trihydrates $Cs_5Zr_4F_{21} \cdot 3H_2O$ and $Rb_5Zr_4F_{21} \cdot 3H_2O$ (Fig. 4, spectra *2*, *3*), it is possible to notice a small low-frequency shift of a number of anion bands in the spectra of the Cs compound, this indicates a less strong binding of the anionic complex to cations Cs^+.

Thermal dehydration of trihydrous Rb- and Cs-crystallohydrates (at 200 °C) does not lead to the formation of anhydrous compounds $M_5Zr_4F_{21}$ ($M = Rb^+, Cs^+$). Bands from a mixture of two phases $MZrF_5$ and M_2ZrF_6 appear in the IR and Raman spectra of heating products. The characteristic bands of 584, 237 cm^{-1} (Rb), 576, 234 cm^{-1} (Cs) from M_2ZrF_6 [27–29] and 557, 400, 264, 205, 182 cm^{-1} (Rb) and 553, 397, 257, 244, 195, 184 cm^{-1} (Cs) from $MZrF_5$.

When the crystallohydrates are heated to temperatures above PT (330, 350 °C), additional bands of low intensity appear against the background of noticeable bands of fluctuations of penta- and hexafluorides in the IR and Raman spectra with maxima at 665 and 668 cm^{-1} for Cs and Rb, respectively, related to stretching νZrO of fragment $Zr_3(\mu_3$–O) oxofluorozirconate $M_2Zr_3OF_{12}$ [20] (Fig. 4, spectra *4*, *5*). The appearance of these bands in the spectra is determined by the onset of pyrohydrolysis of the $MZrF_5$ phases by air moisture. It should be noted that a very weak band at 668 cm^{-1} from the oxofluoride phase is already visible in the spectrum of $Rb_5Zr_4F_{21} \cdot 3H_2O$ sample heated to 270 °C (up to PT), i.e., the hydrolytic decomposition of $RbZrF_5$ begins at lower temperatures than hydrolytic decomposition of $CsZrF_5$ compounds.

Conclusions

The isostructural nature of the crystallohydrates $M5Zr_4F_{21} \cdot 3H_2O$ ($M = Rb^+$, Cs^+) was confirmed based on the affinity of the X-ray diffraction patterns and the similarity of the vibrational (IR, Raman) spectra. It was found that coordinated H_2O molecules participate in the formation of stronger H-bonds of the OH$\cdots$F type in the $Rb_5Zr_4F_{21} \cdot 3H_2O$ structure than in $Cs_5Zr_4F_{21} \cdot 3H_2O$. The vibrational frequencies of the anion $[Zr_4F_{22}(H_2O)_2]^{6-}$ (C_{2h}) are calculated and band attributions are made in experimental spectra based on the results of quantum chemical calculations of the model cluster $[Cs_{12}Zr_4F_{24}(H_2O_2)]^{4+}$]. The results obtained are useful in the comparative evaluation of vibrational spectra in the series of fluoride metal crystallohydrates with variations in the molar ratios F/M(IV) and H_2O/M(IV) and materials based on them.

It was found that the thermal dehydration of $Cs_5Zr_4F_{21} \cdot 3H_2O$ and $Rb_5Zr_4F_{21} \cdot 3H_2O$ proceeds in one stage. The dehydration process is coupled in temperature with thermolysis and the formation of two thermally more stable compounds $MZrF_5$ and M_2ZrF_6. Rubidium and caesium pentafluorocyrconates $MZrF_5$, obtained by decomposition of $M_5Zr_4F_{21} \cdot 3H_2O$, are not isostructural phases.

Funding

The study was conducted with the financial support of the Ministry of Education and Science (state task FWFN-2025-0005).

Conflict of interest

The authors declare that they have no conflict of interest.

References

[1] R.D. Shannon. Acta Crystallogr., Sect. A., **32**, 751 (1976). DOI: 10.1107/S0567739476001551

[2] H. Bode, G. Teufer. Z. anorg. allg. Chem., **283** (1–6), 18 (1956). DOI: 10.1002/zaac.19562830105

[3] V.R. Hoppe, D. Mehlhorn. Z. anorg. allg. Chem., **425** (3), 200 (1976). DOI: 10.1002/zaac.19764250303

[4] A.V. Gerasimenko, I.A. Tkachenko, V.Ya. Kavun, N.A. Didenko, V.I. Sergienko. Russ. J. Inorg. Chem., **51** (1), 9 (2006). DOI: 10.1134/S0036023606010037.

[5] A. Zalkin, D. Eimerl, S.P. Velsko. Acta Cryst., **44C** (12), 2050 (1988). DOI: 10.1107/S0108270188008303

[6] B.V. Bukvetskiy, A.V. Gerasimenko, R.L. Davidovich. Koord. khimiya, **17** (1), 35 (1991) (in Russian).

[7] F. Gabela, B. Kojić-Prodić, M. Šljukić, Ž. Ružic-Toroš. Acta Cryst., **B33** (12), 3733 (1977). DOI: 10.1107/S0567740877011960

[8] B. Kojić-Prodić, F. Gabela, Ž. Ružić-Toroš, M. Šljukić. Acta Cryst., **B37**, 1963 (1981). DOI: 10.1107/S0567740881007772

[9] Chr. Neumann, H. Saalfeld. Z. Kristallogr., **175** (3), 177 (1986). DOI: 10.1524/zkri.1986.175.14.177

[10] V.V. Tkachev, A.A. Udovenko, R.L.Davidovich, L.O. Atovmyan. Koord. khimiya, **17** (12), 1635 (1991) (in Russian).

[11] V.V. Tkachev, R.L.Davidovich, L.O. Atovmyan. Koord. khimiya, **18** (1), 38 (1992) (in Russian).

[12] V.V. Tkachev, R.L.Davidovich, L.O. Atovmyan. Koord. khimiya, **18** (1), 42 (1992) (in Russian).

[13] A.V. Gerasimenko, I.A. Tkachenko, V.Ya. Kavun, N.A. Didenko. V sb.: *Sbornik trudov III Mezhdunarodnogo sibirskogo seminara ISIF–2008 po himii i tekhnologii sovremennyh neorganicheskih ftoridov*, pod red. V.Ya. Kavuna, Yu.L. Hromovoj (Reya, Vladivostok, 2008). P. 158 (in Russian).

[14] R.L. Davidovich, V.B. Logvinova, L.V. Teplukhina. Koord. khimiya, **18** (1), 48 (1992) (in Russian).

[15] M.M. Godneva, D.L. Motov. *Khimiya podgruppy titana. Sul'faty, ftoridy, ftorosul'faty iz vodnyh sred* (Nauka, M., 2006). p. 302 (in Russian).

[16] R.L. Davidovich, T.A. Kaidalova, T.F. Levchishina, V.I. Sergienko. *Atlas infrakrasnyh spektrov pogloshcheniya i rentgenometricheskih dannyh kompleksnyh ftoridov metallov IV i V grupp* (Nauka, M., 1972). p. 252 (in Russian).

[17] M.W. Schmidt, K.K. Baldridge, J.A. Boatz, S.T. Elbert, M.S. Gordon, J.H. Jensen, S. Koseki, N. Matsunaga, K.A. Nguyen, S. Su, T.L. Windus, M. Dupuis, J.A. Montgomery. J. Comput. Chem., **14**, 1347 (1993). DOI: 10.1002/jcc.540141112

[18] I.V. Tananaev, L.S. Guzeeva, K.I. Petrov. Izv. SO AN SSSR, ser. him. nauk, **1** (2), 103 (1968) (in Russian).

[19] D. Köller, B.D. Müller. Z. Anorg. Allg. Chem., **628**, 575 (2002). DOI: 10.1002/1521-3749(200203)628:3%3C575::AID-ZAAC575%3E3.0.CO;2-L

[20] E.I. Vojt, N.A. Didenko ZHurn. neorg. himii, **69** (12), 69 (2024) (in Russian). DOI: 10.31857/S0044457X24120063

[21] V. Gaumet, M. El-Ghozzi, D. Avignant. Eur. J. Solid State Inorg. Chem., **34** (3), 283 (1997). DOI: 10.1002/CHIN.199738010

[22] Yu.M. Korenev, V.V. Govorov, A.A. Kosorukov, R. Riyazur, A.V. Novoselova. Izv. SO AN SSSR, ser. him. nauk, **1** (2), 10 (1968) (in Russian).

[23] G.D. Robbins, R.E. Thoma, H. Insley. J. Inorg. Nucl Chem., **27**, 559 (1965). DOI: 10.1016/0022-1902(65)80261-5

[24] D. Avignant, I. Mansouri, R. Chevalier, J. Cousseins J. Solid State Chem., **38** (1), 121 (1981). DOI: 10.1016/0022-4596(81)90481-3

[25] E.Yu. Yanson, Ya.K. Putnin. *Teoreticheskie osnovy analiticheskoj himii* (Vysshaya shkola, M., 1980). p. 260 (in Russian).

[26] N.A. Didenko, E.I. Voit, K.A. Sayankina, A.V. Gerasimenko, A.B. Slobodyuk. Vestnik DVO RAN, **5**, 107 (2021) (in Russian). DOI: 10.37102/0869-7698_2021_219_05_09

[27] I.W. Forrest, A.P. Lane. Inorganic Chemistry, **15** (2), 265 (1976). DOI: 10.1021/ic50156a004

[28] A.P. Lane, D.W.A. Sharp. J. Chem. Soc. A, **2942** (1969). DOI: 10.1039/J19690002942

[29] L.M. Toth, J.B. Bates. Specrochim. Acta, **30A**, 1095 (1974). DOI: 10.1016/0584-8539(74)80025-5

Translated by A.Akhtyamov